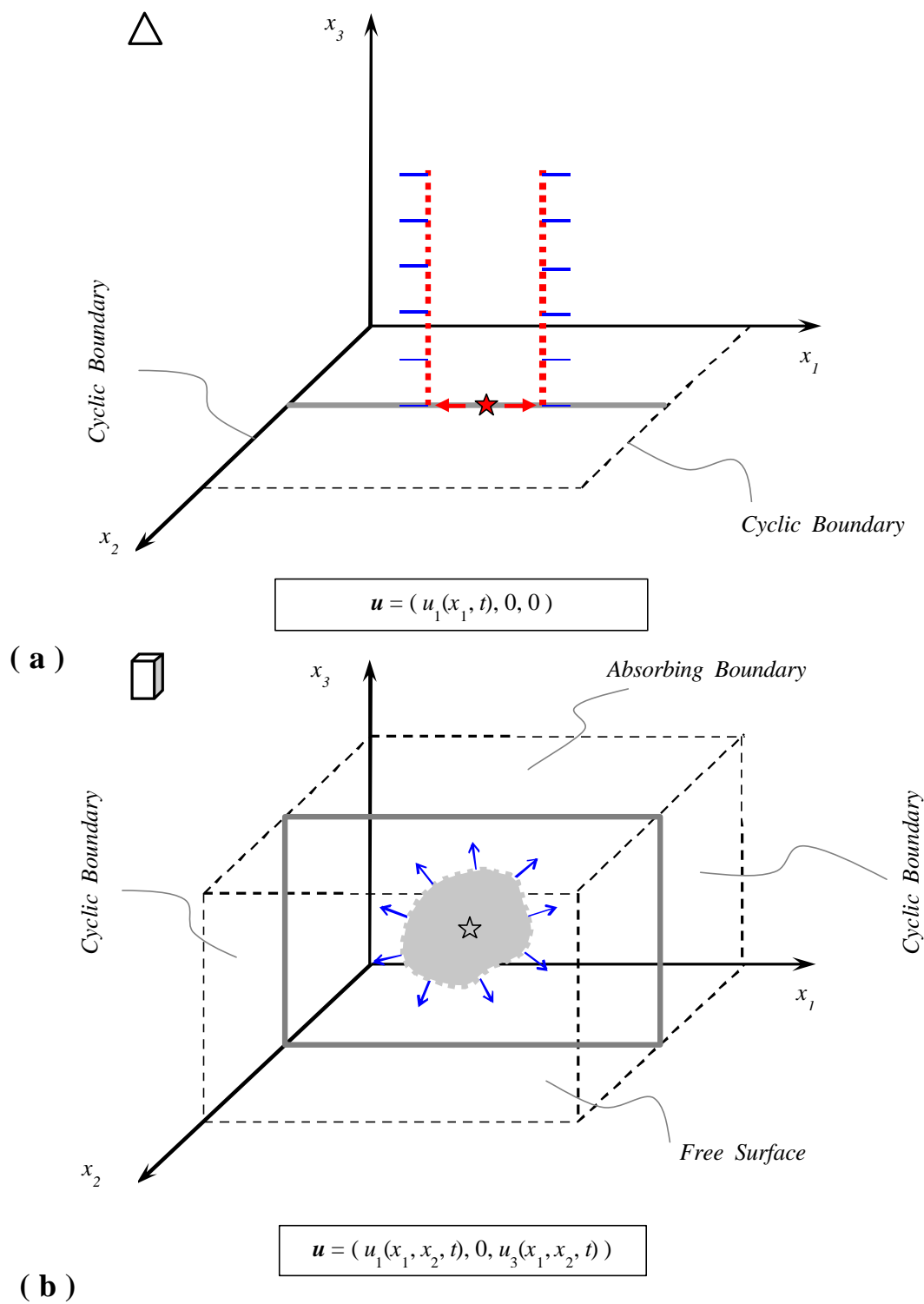
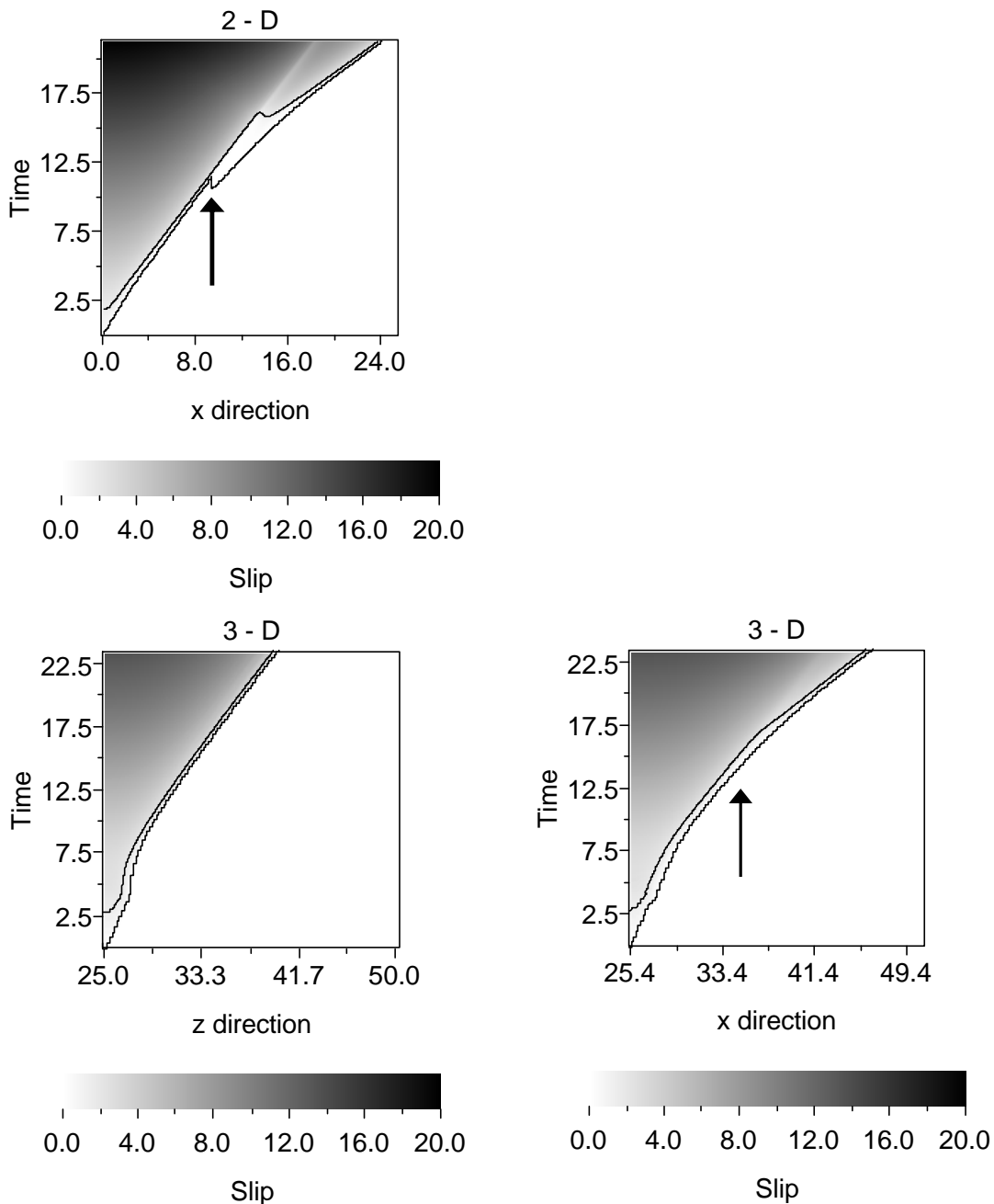


## Figures of Chapter 4



**Figure 4.1.** Schematic representation the geometry of the FD numerical codes. In the 2 – D model ( a ) the rupture enlarges in the  $x_1$  direction and all the solutions are independent on the  $x_2$  coordinate; only the 1 – components of the solutions are non null. In the 3 – D model ( b ) a vertical fault is represented. All the solutions have two non null components and each component depends on two spatial coordinates. In each panel the fundamental building block is represented: an equilateral triangle for 2 – D model and a parallelepiped for 3 – D model.



**Figure 4.2.** Comparison between slip as a function of space and time, obtained from numerical results for 2 – D fault, ( a ), and 3 – D vertical fault, ( b ) and ( c ), obeying to classical slip – weakening constitutive law. The cohesive zone is indicated on each panel and the time of crack tip bifurcation is marked by a vertical arrow. For the 3 – D model panel ( b ) shows the slip as a function of  $x_3$  and  $t$ , panel ( c ) shows the slip as a function of  $x_1$  and  $t$ .

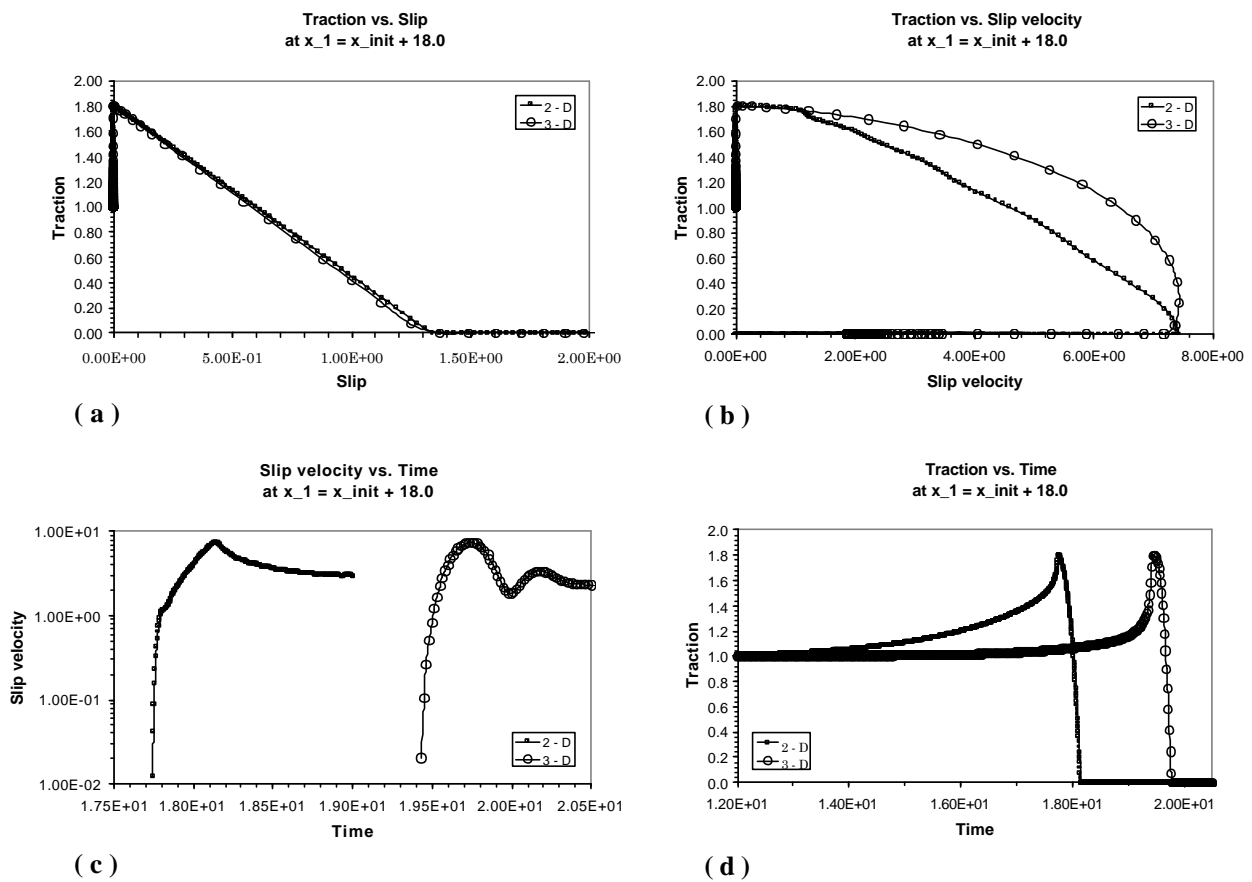


**Figure 4.3.** Slip – weakening curves ( a ), phase portrait ( b ), slip velocity history in log – scale and traction history ( d ) for 2 – D ( black square ) and for 3 – D ( open circles ) models. All the solution are calculated in the point along the  $x_1$  axis and at a distance of 18 units from the nucleation point. All the parameter are the same of those used in Figure 4.1, and they are listed in Table 4.1.

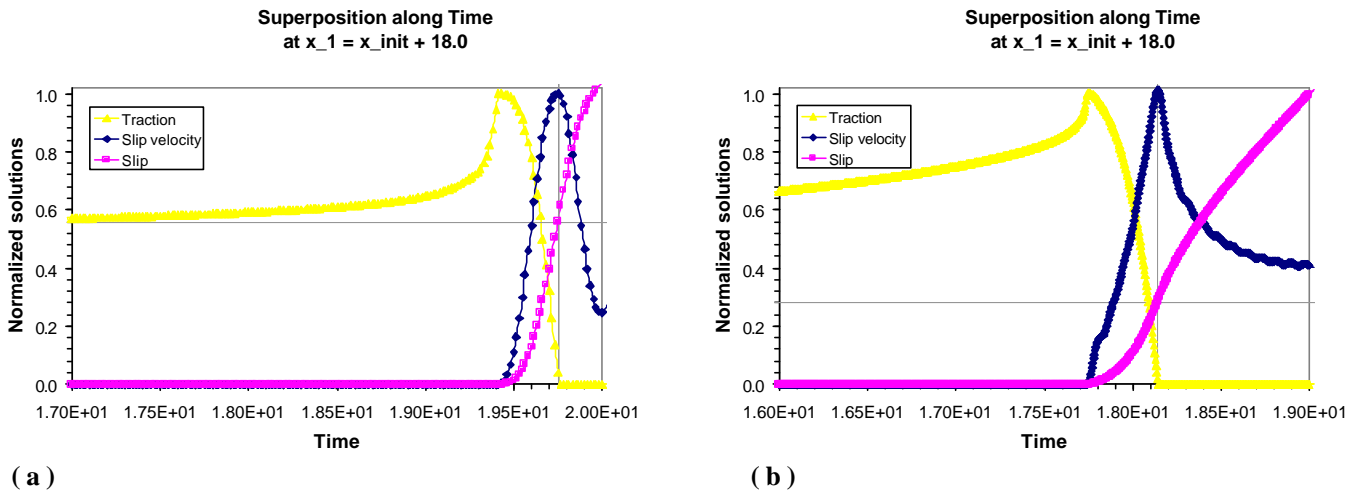


**Figure 4.4.** Superposition in time of total dynamic traction, slip velocity and slip for 3 – D ( a ) and 2 – D model ( b ) in the same point used if Figure 4.3. All quantities are normalized to the each maximum values within the time windows. A grey horizontal line indicates in each panel the normalized characteristic slip – weakening distance, while a vertical grey lines marks the time step at which the normalized friction reaches the kinetic frictional level. We emphasize that in both fault model such an instant is the time step at which the slip velocity is at its maximum value.

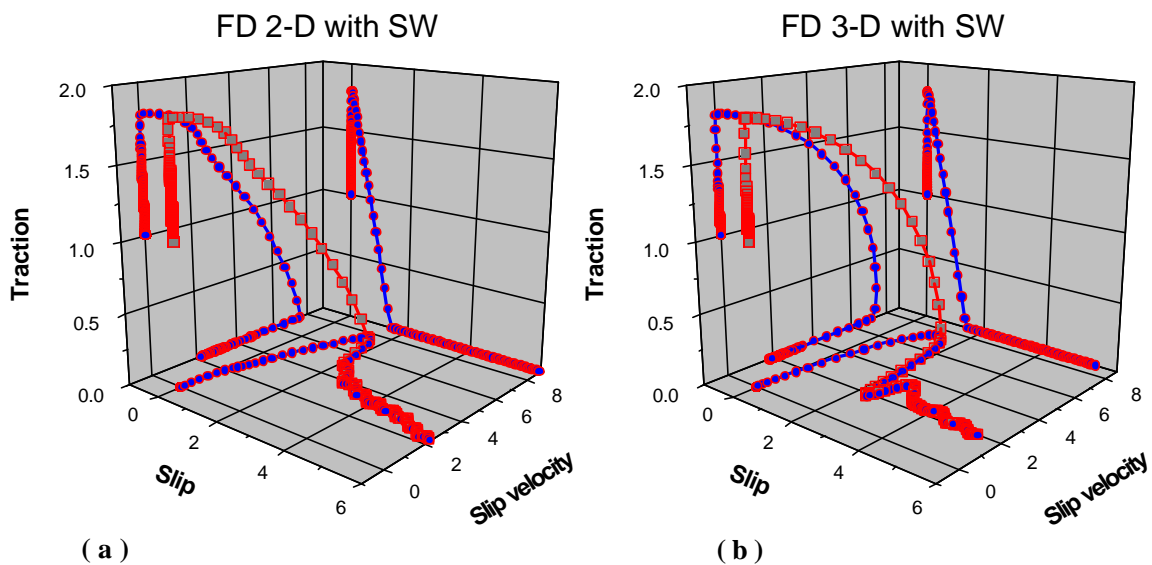




**Figure 4.5.** Tri – dimensional trajectories of total dynamic traction as a function of slip and slip velocity obtained from numerical simulation for a 2 – D ( a ) and a 3 – D model ( b ). In each panel we project the trajectory on the slip – weakening plane, on the phase plane ( i. e. traction vs. slip velocity ) and on the slip – slip velocity plane.

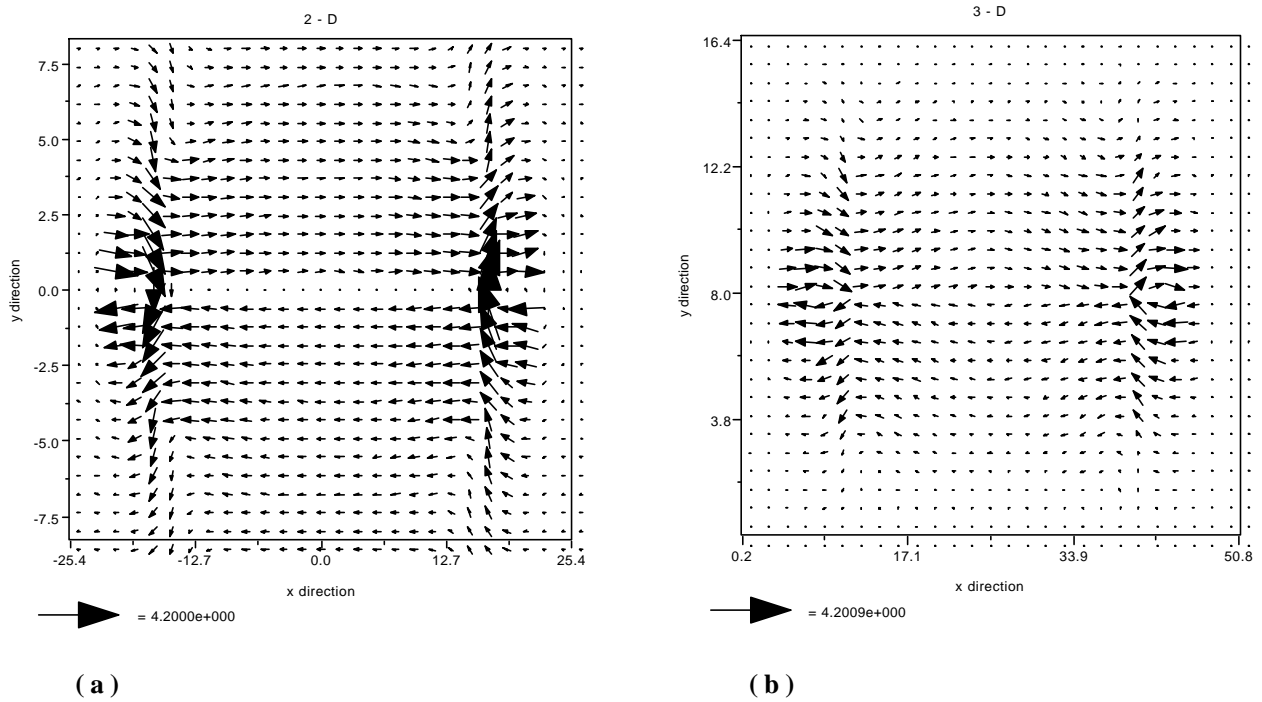


**Figure 4.6.** Vector plot representing the slip velocity vector in an horizontal plane, perpendicular to the fault plane ( see Figure 4.1 ). For the 2 – D model ( a ) the fault line is located at  $x_2 = 0$ , while for the 3 – D model ( b ) it is located at  $x_2 = 8.0$ .

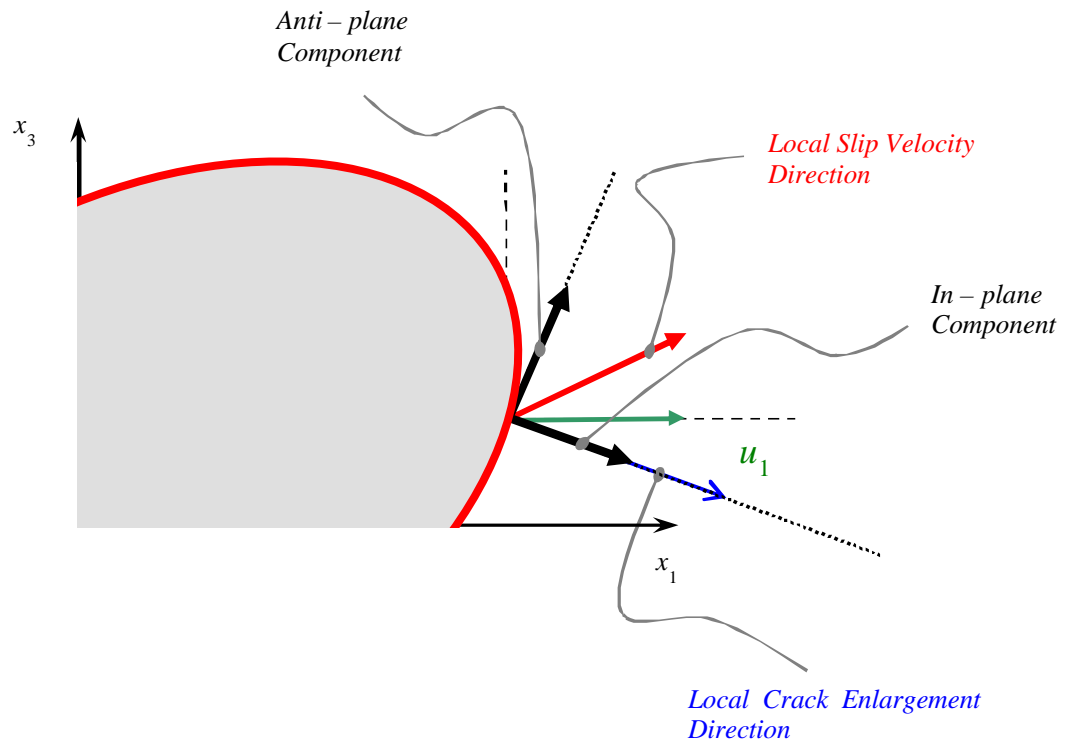
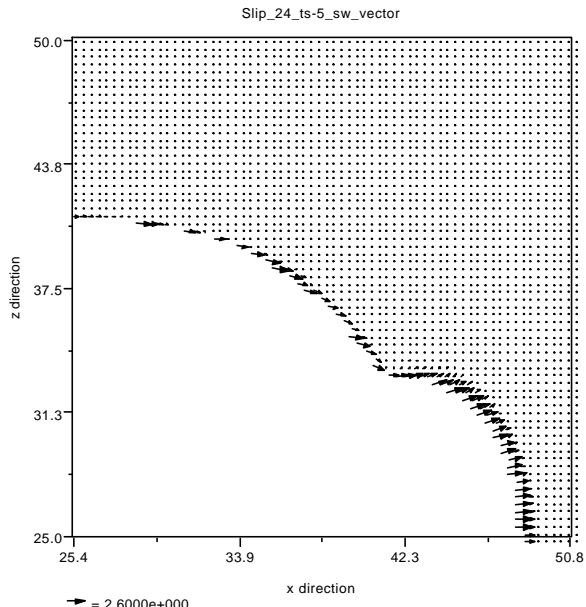
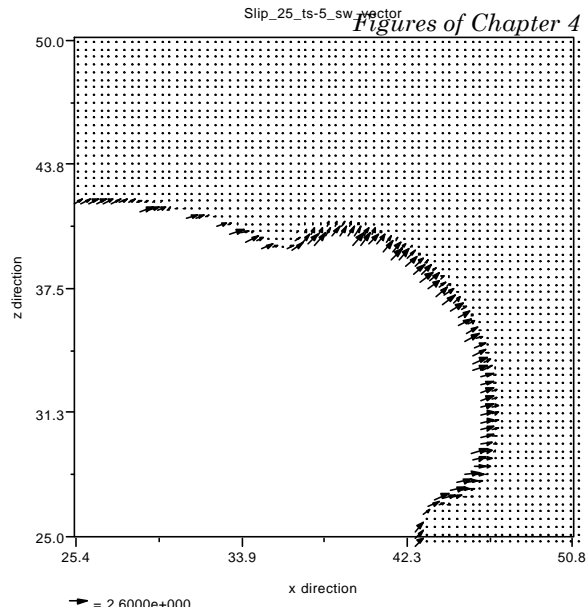


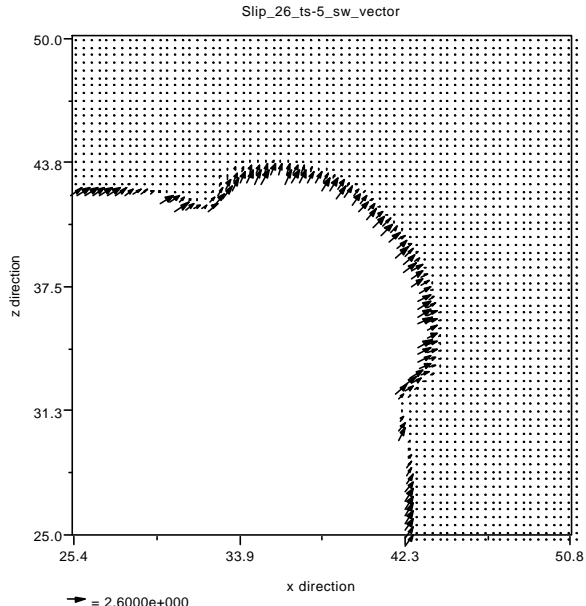
**Figure 4.7.** Schematic representation of an instantaneous position of the crack tip ( solid red line ). The solid red arrow indicates the local, instantaneous slip velocity vector; the blue arrow represents the local, instantaneous crack enlargement direction; the black arrows represent the pure in – plane and pure anti – plane modes of propagation. They are, by definition, collinear and perpendicular to the local, instantaneous crack tip enlargement direction. They do not coincide, in full of generality, with the components 1 and 2 of the slip velocity ( green arrows ). The star marks the location of the nucleation point.



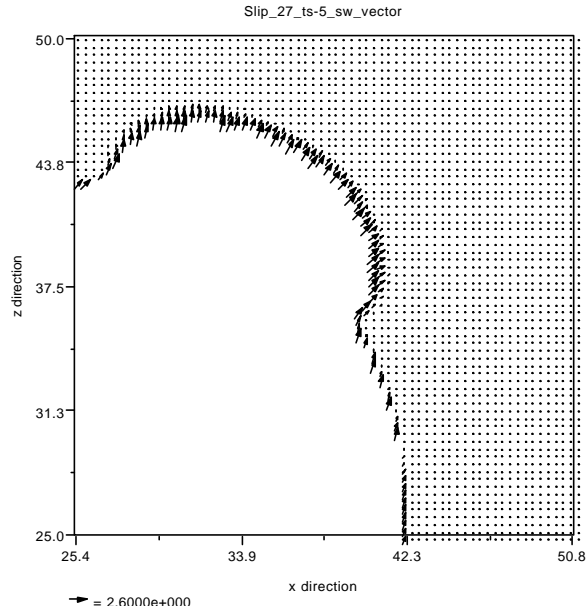
(a)



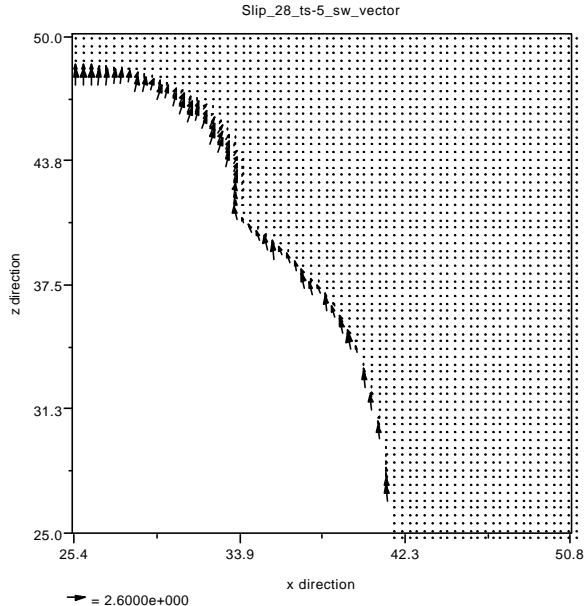
(b)



(c)

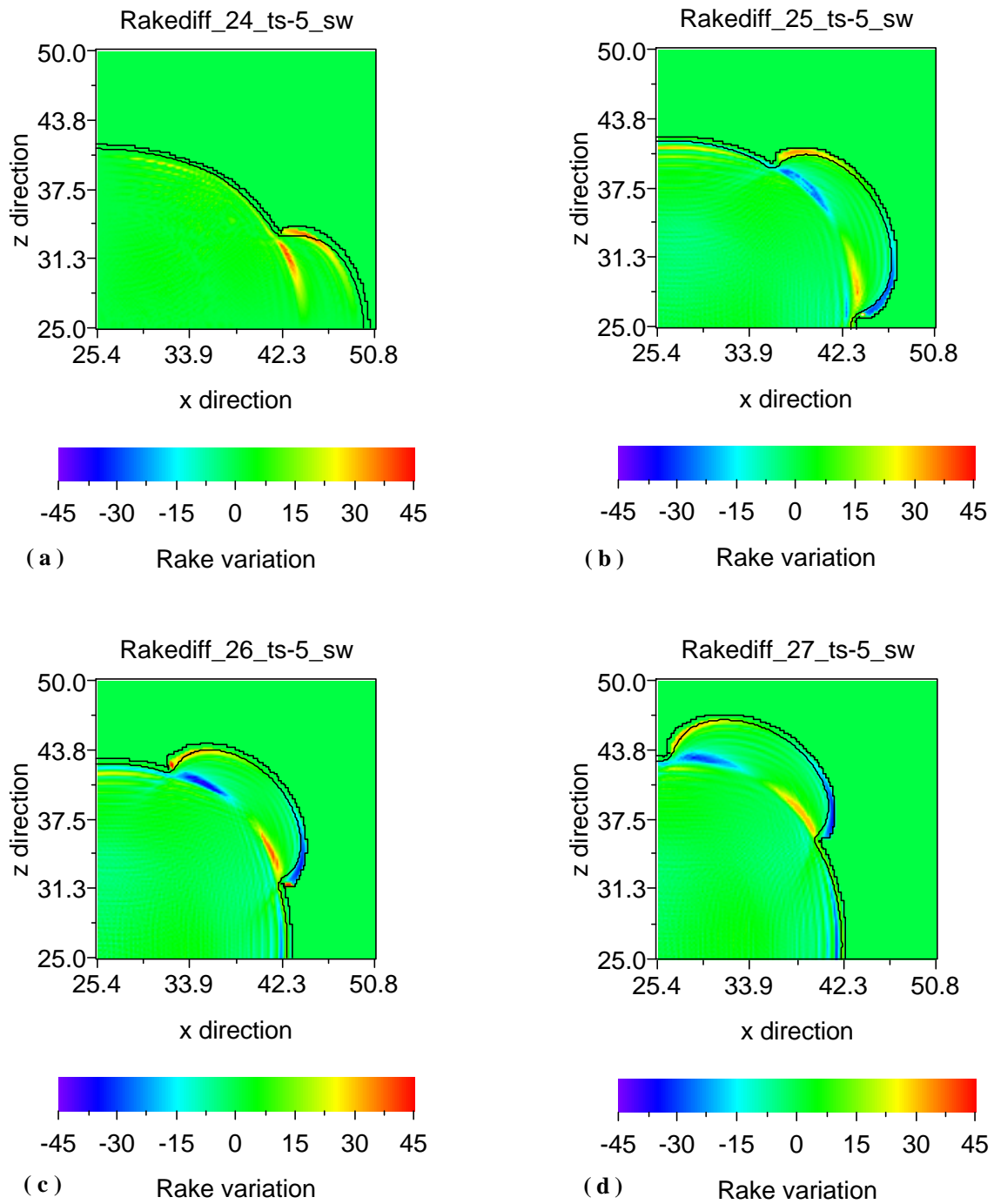


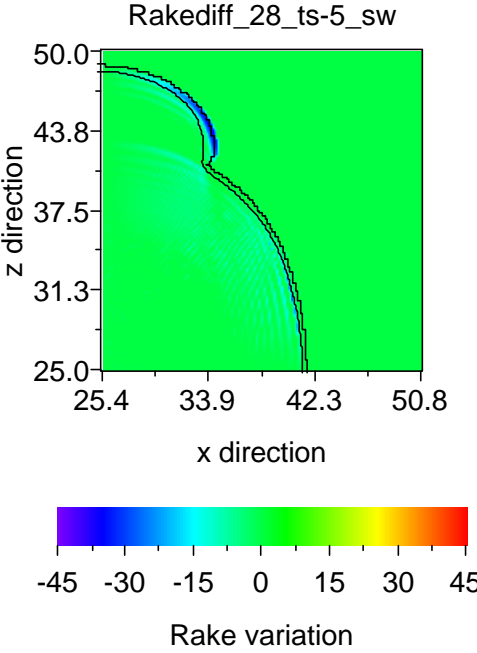
(d)



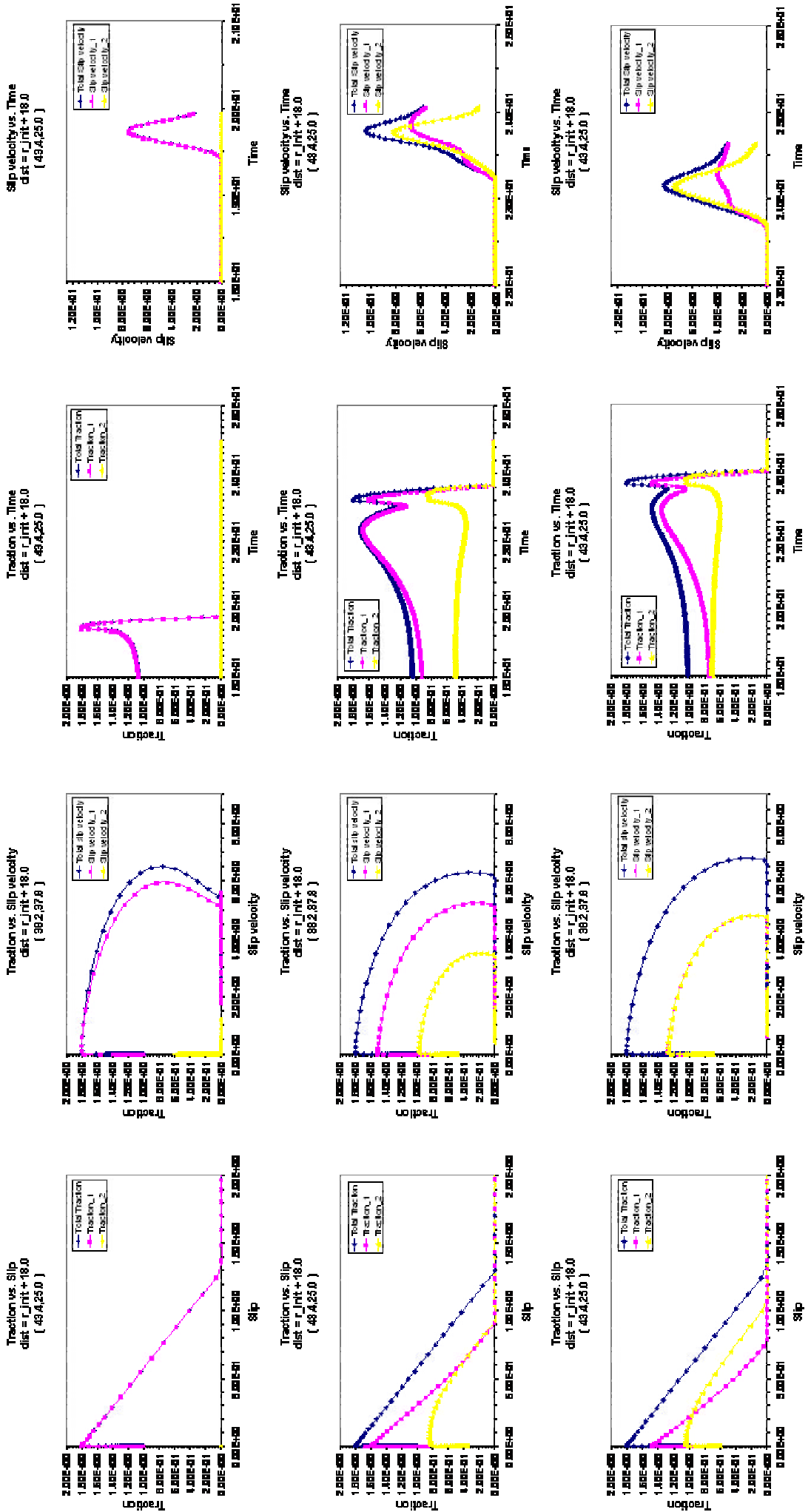
(e)

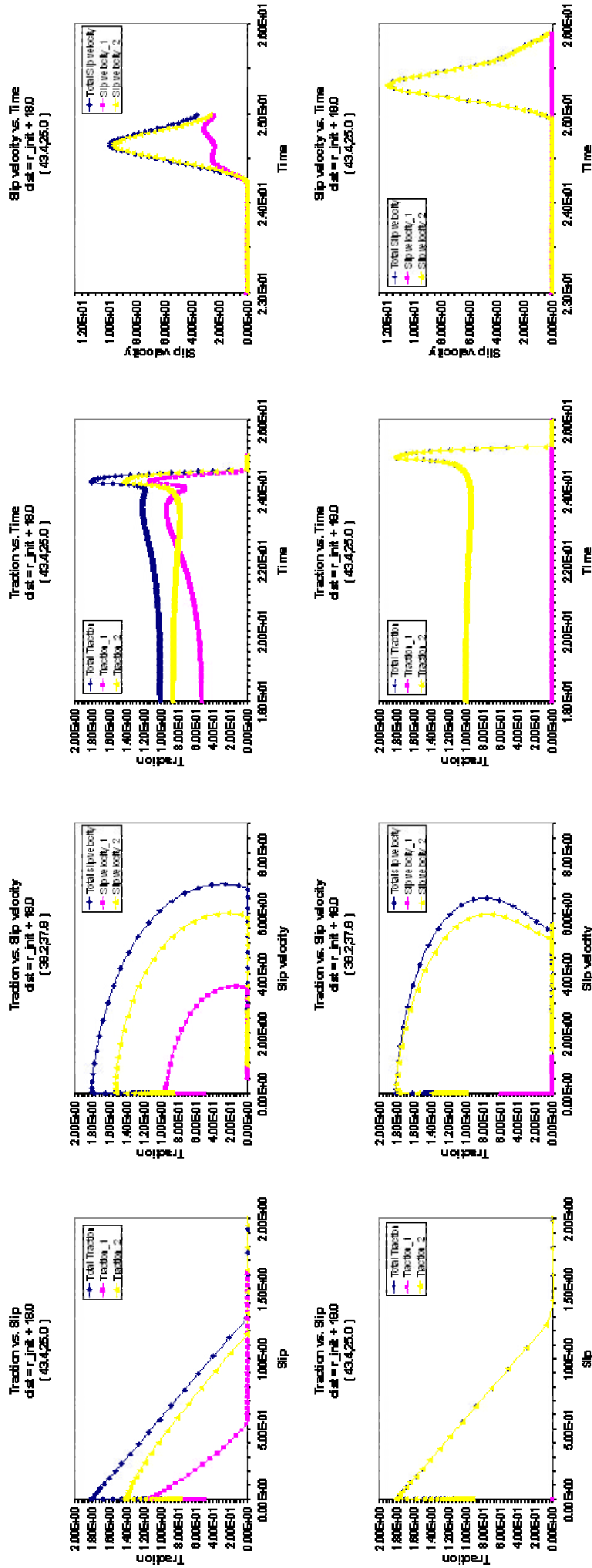
**Figure 4.8.** Vector plots representing the slip within the cohesive zone for five different initial traction direction: 0 degrees ( formally pure in – plane initial mode, a ), 30 ( b ), 45 ( c ), 60 ( d ), 90 degrees ( formally pure anti – plane initial mode, e ). Plots are made for the last time step.



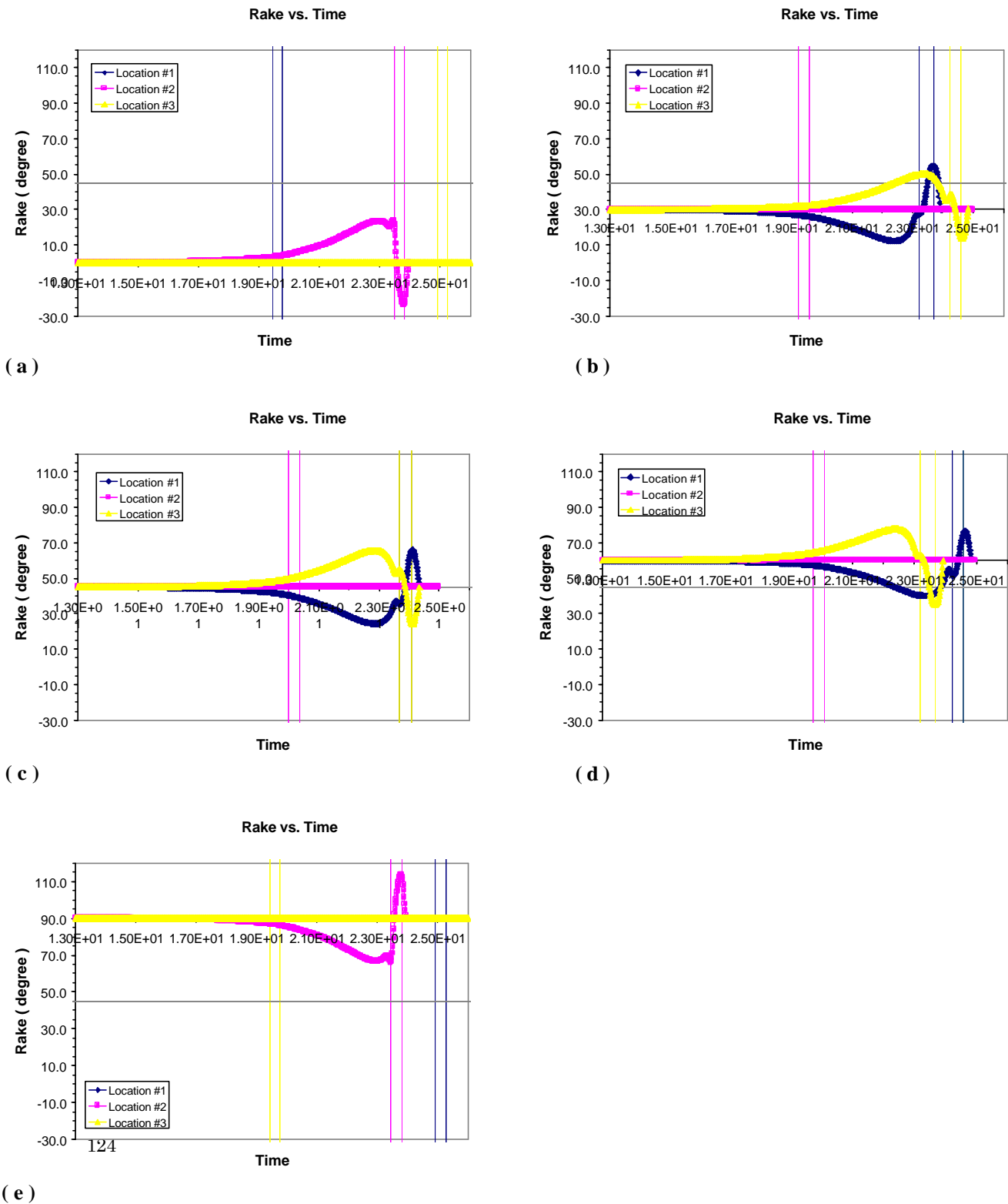


**Figure 4.9.** Differences between modelled rake and initial rake for the fives configurations reported in Figure 4.8, at the final time step. We indicate with black lines the extension of the cohesive zone.



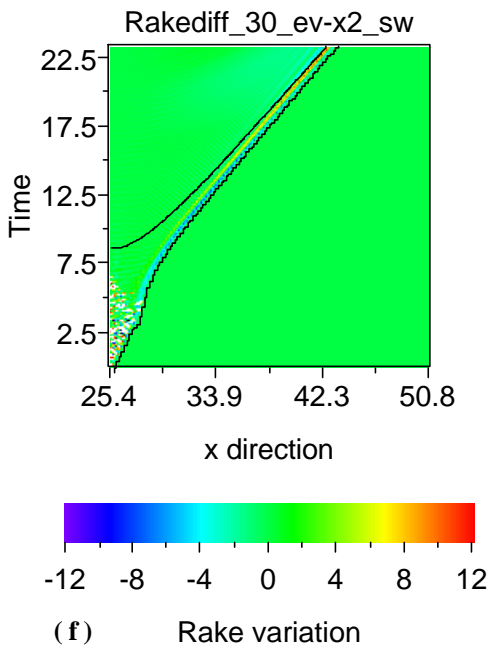
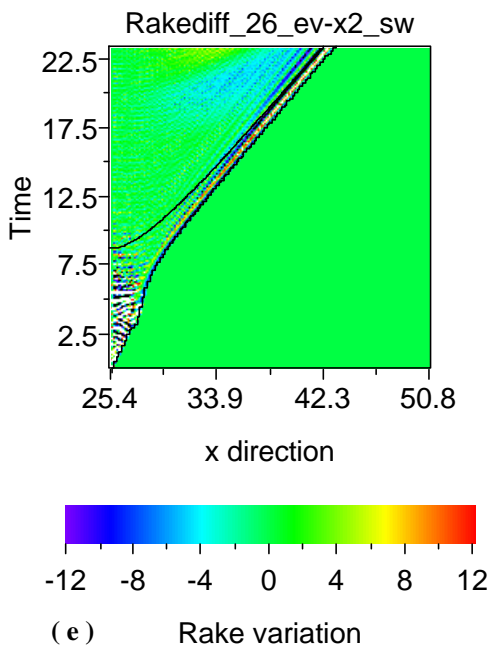
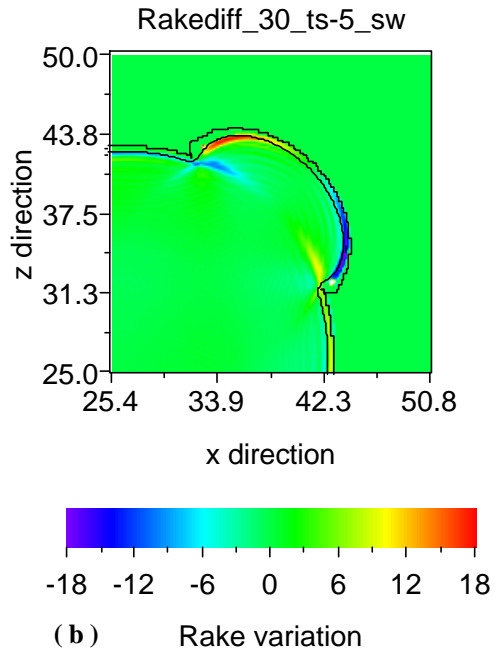
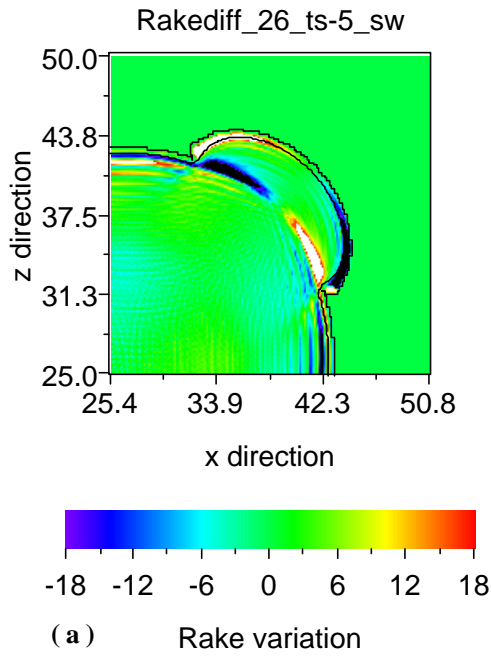


**Figure 4.10.** Slip – weakening curves, phase diagrams, traction histories and slip velocity histories for different cases of Figures 4.8 and 4.9, Each row is for the same initial rake and both 1 and 3 components are plotted in each panel.





**Figure 4.11.** Behaviour of rake ( in degree ) vs. time for different five cases of Figures 4.8, 4.9 and 4.10. In each panel are represented the rake history at three different locations at a distance of 18.0 units from the nucleation point: location #1 refers is in the  $x_1$  axis, location #3 is in the  $x_3$  axis while location #2 is in the direction of the initial rake. Horizontal grey lines indicate the initial rake value, for each configuration; each couple of vertical lines represent the temporal extension of the cohesive zone, for each locations. The first line indicates the time step at which the traction is at ht upper yield stress, while the second one indicates the time step at which the friction level is reached ( and the fault has slipped by an amount equal to the characteristic slip – weakening distance ).



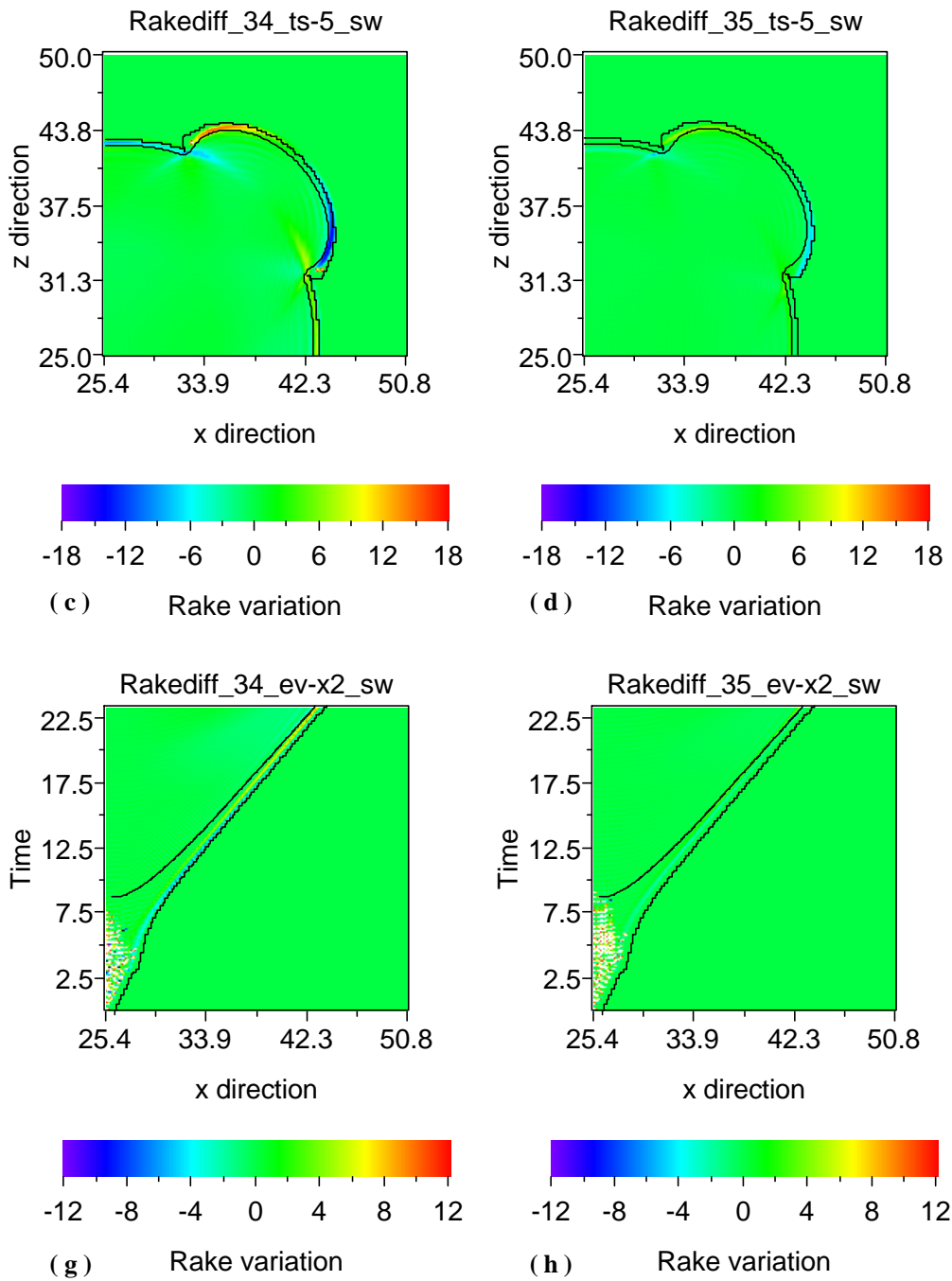


**Figure 4.12.** Rake variation at the final time step in the fault plane ( a, b, c and d ) and rake variation as a function of the 1 coordinate and of the time ( e, f, g and h ). In all panels the cohesive zone is indicated. Input parameters are in Table 4.2.

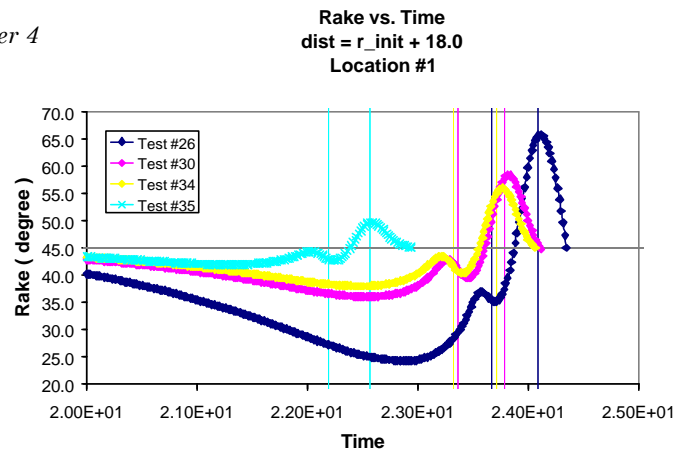


**Figure 4.13.** Rake histories in a point located along the  $x_1$  axis and at a distance of 18.0 units from the nucleation point. The initial rake is of 45 degrees. Vertical lines indicate, as usual, the start and the end of breakdown zone, for all the four cases in which the strength parameter  $S$  is equal to 0.8, but the absolute values of frictional parameters is varying, as described in Table 4.3.

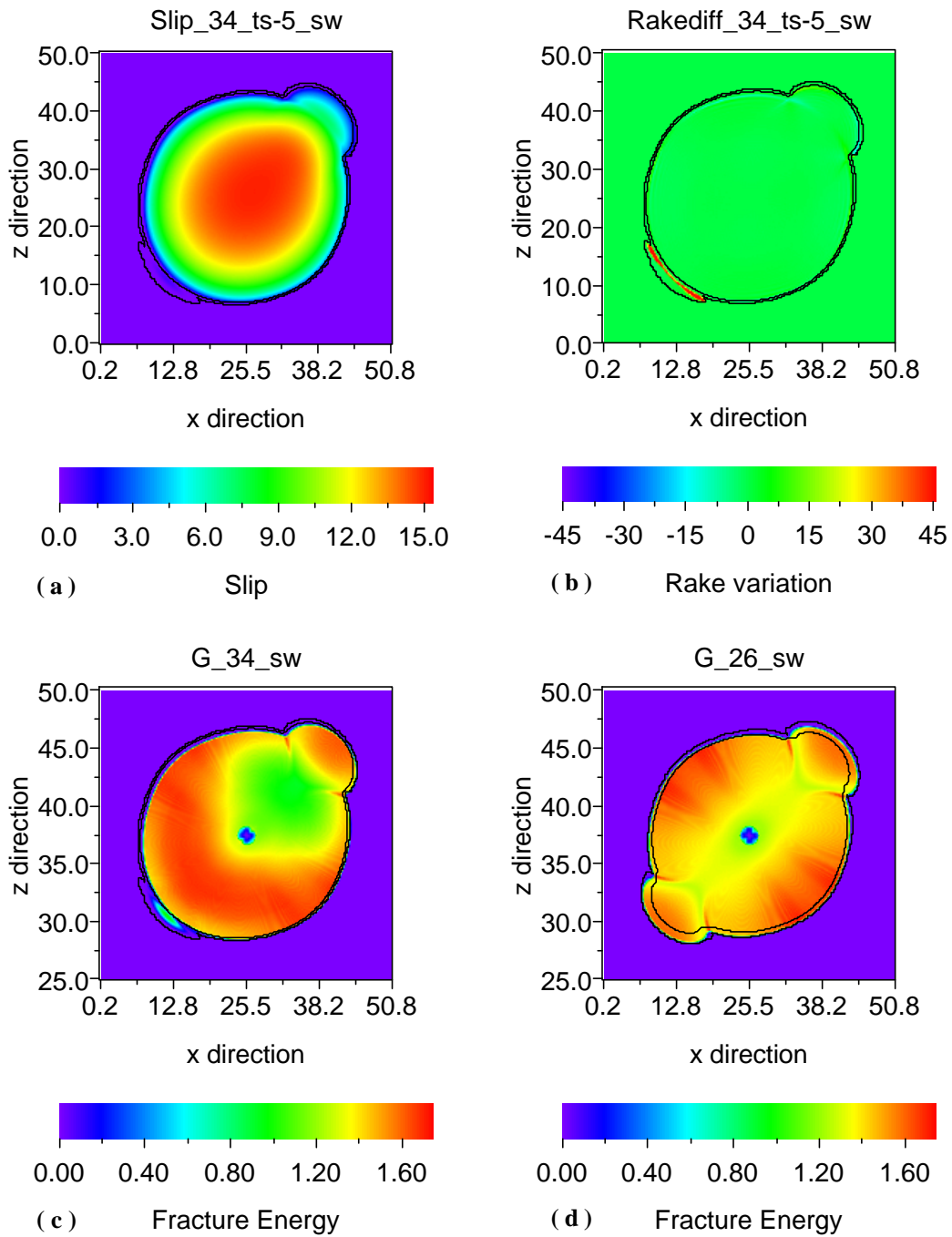


**Figure 4.14.** Slip ( a ), rake variation and fracture energy  $G$  ( c ) in the fault plane for the configuration #34 of Figure 4.13. Fracture energy of the reference case ( #26, panel d ) is reported for completeness. We also indicate the spatial extension of the cohesive zone.

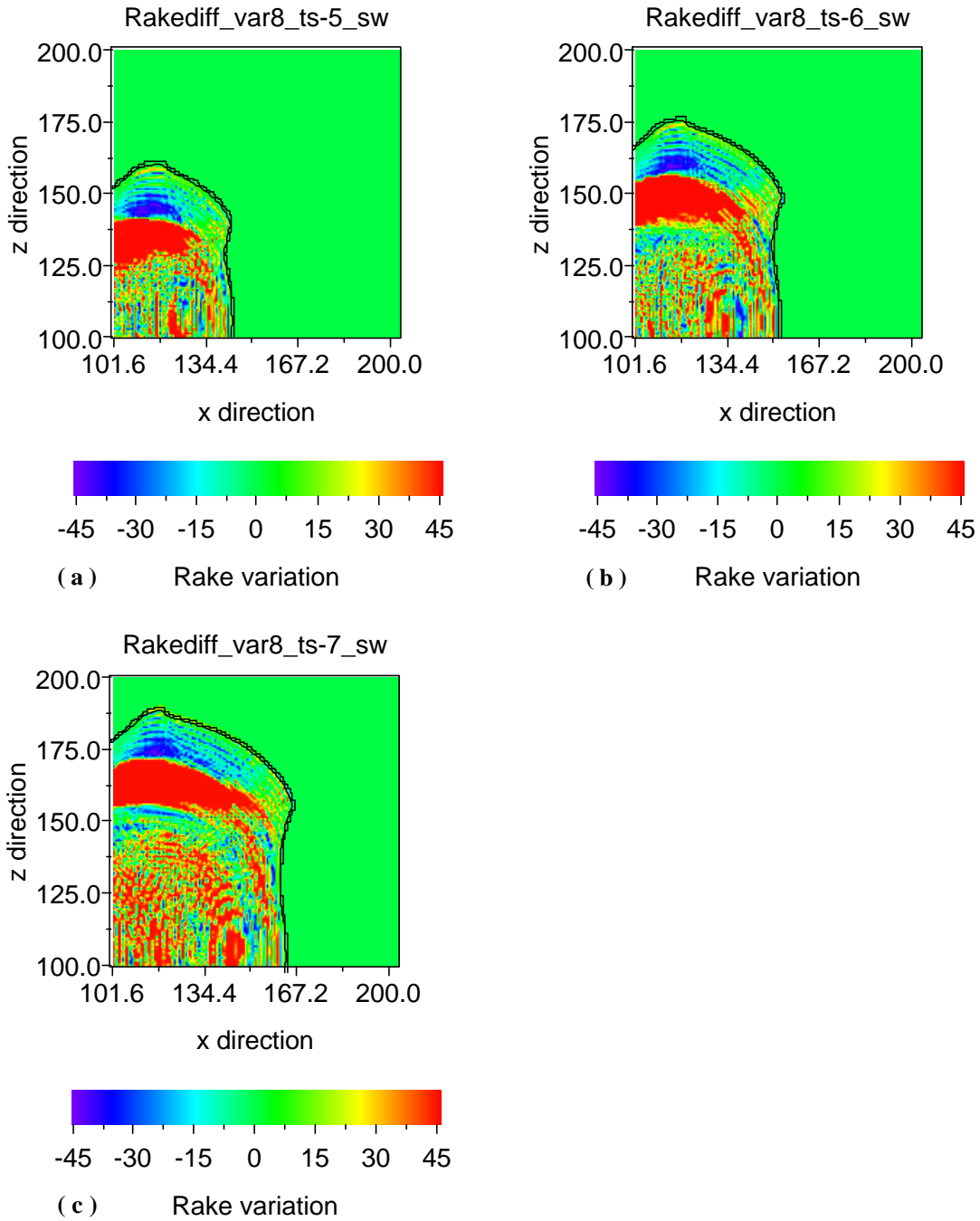


**Figure 4.15.** Rake variation on the fault plane for three different time step for an heterogeneous configuration in which a barrier with  $S = 2.0$  is located at  $x_1 = 124.6$ .

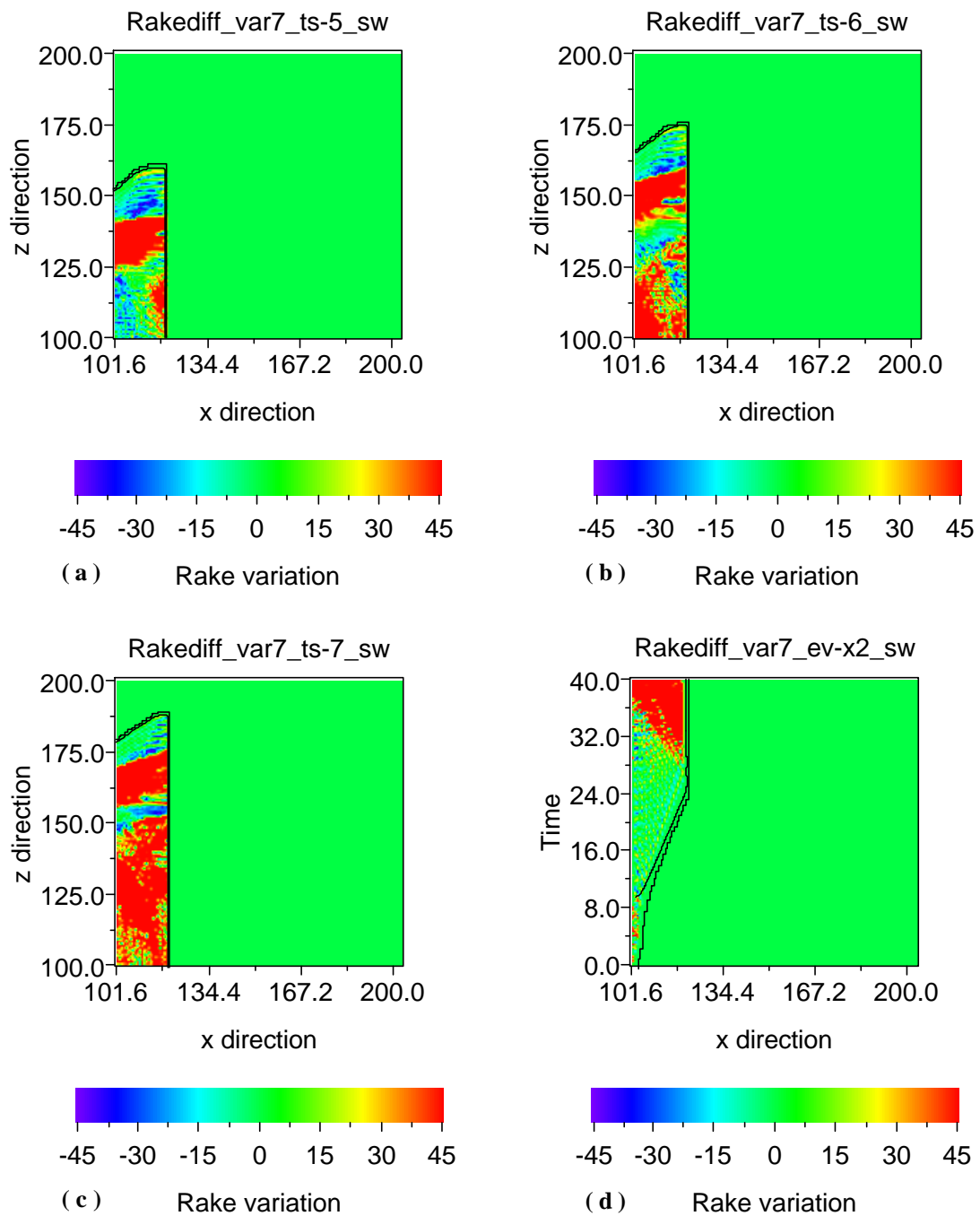


**Figure 4.16.** Rake variation in the fault plane for an heterogeneous configuration in which a barrier with  $S = 19.0$  is located at  $x_1 = 124.6$ .